Parameter identification of a nonlinear model: replicating the motion response of an autonomous underwater vehicle for dynamic environments

6 authors, including:

Supun Randeni
Massachusetts Institute of Technology
10 PUBLICATIONS **42** CITATIONS

SEE PROFILE

Alexander LeBaron Forrest
University of California, Davis
86 PUBLICATIONS **568** CITATIONS

SEE PROFILE

Remo Cossu
The University of Queensland
24 PUBLICATIONS **60** CITATIONS

SEE PROFILE

Zhi Quan Leong
University of Tasmania
68 PUBLICATIONS **275** CITATIONS

SEE PROFILE

Some of the authors of this publication are also working on these related projects:

Project Cornerstone View project

Fluid Structure Interaction - Prediction of Sea-loads on ship hull structures View project

CrossMark

ORIGINAL PAPER

Parameter identification of a nonlinear model: replicating the motion response of an autonomous underwater vehicle for dynamic environments

S. A. T. Randeni P. · **A. L. Forrest** ·
R. Cossu · **Z. Q. Leong** · **D. Ranmuthugala** ·
Val Schmidt

Abstract This study presents a system identification algorithm to determine the linear and nonlinear parameters of an autonomous underwater vehicle (AUV) motion response prediction mathematical model, utilising the recursive least squares optimisation method. The key objective of the model, which relies solely on propeller thrust, gyro measurements and parameters representing the vehicle hydrodynamic, hydrostatic and mass properties, is to calculate the linear velocities of the AUV in the x, y and z directions. Initially, a baseline mathematical model that represents the dynamics of a *Gavia* class AUV in a calm water environment was developed. Using a novel technique developed in this study, the parameters within the baseline model were calibrated to provide the motion response in different environmental conditions by conducting a calibration mission in the new environment.

The accuracy of the velocity measurements from the calibrated model was substantially greater than those from the baseline model for the tested scenarios with a minimum velocity prediction improvement of 50%. The determined velocities will be used to aid the inertial navigation system (INS) position estimate using a Kalman filter data fusion algorithm when external aiding is unavailable. When an INS is not externally aided or constrained by a mathematical model such as that presented here, the positioning uncertainty can be more than 4% of the distance travelled (assuming a forward speed of $1.6\,\mathrm{m\,s^{-1}}$). The calibrated model is able to compute the position of the AUV within an uncertainty range of around 1.5% of the distance travelled, significantly improving the localisation accuracy.

Keywords Autonomous underwater vehicles (AUVs) · System identification · Recursive least squares optimisation · Mathematical models · Underwater localisation · Model-aided inertial navigation system

S. A. T. Randeni P. (✉)· A. L. Forrest · R. Cossu ·
Z. Q. Leong · D. Ranmuthugala
Australian Maritime College, University of Tasmania,
Launceston, Australia
e-mail: Supun.Randeni@utas.edu.au

A. L. Forrest
Department of Civil and Environmental Engineering,
University of California – Davis, One Shields Ave, Davis,
CA 95616, USA

R. Cossu
School of Civil Engineering, University of Queensland,
Brisbane, Australia

V. Schmidt
Centre for Coastal and Ocean Mapping, University of New
Hampshire, Durham, NH 03824, USA

1 Introduction

Autonomous underwater vehicles (AUVs) have evolved as specialised tools for challenging commercial, scientific, and military underwater applications such as subsea inspections [1], characterisation of the midwater column [2] and security exercises in unstructured environments [3]. Despite the developments of AUVs

Springer

reaching back to the 1970s, the navigation and control subsystems of AUVs are continuously undergoing improvements [4]. In particular, one of the main challenges is accurate localisation and navigation in blue water (i.e. operating in regions out of range of bottom-track-aided navigation), and to achieve the dynamic control stability of the vehicle that determines the data quality of AUV surveys [3].

Inertial navigation systems (INS) are one of the key methods to localise and navigate AUVs. An INS determines the position, velocity and orientation of the vehicle using data from inertial measurement units (IMUs) relative to inertial space. Due to inherent errors, the INS localisation solution in its free inertial mode (i.e. unaided-INS) rapidly drifts unless it is externally aided with vehicle's speed over the ground measurements from a bottom tracking Doppler velocity log (DVL) [5,6]. When DVL aiding is intermittently or completely unavailable (for example, due to instrument noise or as a result of the vehicle-to-seabed distance being larger than the transmission range of acoustic frequency associated with the DVL), the vehicle velocities can be approximated with a mathematical model that characterises the hydrostatic and hydrodynamic properties of the AUV; i.e. a model-aided INS [7,8]. Although the localisation solution from a model-aided INS is not as accurate as a DVL-aided INS, its accuracy is better than the unaided INS and the water-track mode of the DVL-aided INS [9].

The velocity response predicting capability of a mathematical model depends on the precision of the parameters representing hydrodynamic, hydrostatic, environmental and external forces, and the mass properties of the AUV, which typically vary with the operating environment and the vehicle configuration (i.e. the trim and ballast conditions). Therefore, a baseline mathematical model with parameters representing a calm water environment may not adequately predict the velocities of an AUV that operates in a dynamic environment in the presence of high currents [10]. An improvement in the velocity prediction is essential to increase the AUV localisation accuracy from a model-aided INS.

A dynamically stable control system is essential for AUVs to undertake challenging tasks in complex flow conditions in high turbulent environments [11], in close proximity to the seabed [12], or to other moving underwater vehicles [13] and near the free surface [14]. AUV control systems can be pre-optimised using a mathematical model that represents the dynamics of an AUV in its anticipated operating water column. With the availability of a mathematical model that updates in real time to characterise the operational environment, the control system optimisation can be conducted in real time or near real time [15].

Mathematical models can additionally be used to accurately predict the vehicle motion response which, in turn, is crucial for several other applications. For example, the velocity components of a turbulent water column can be determined through a non-acoustic technique using the AUV motion response, as previously described by the authors as the WVAM method in Randeni et al. [11]. The WVAM method uses a mathematical model to calculate the flow velocities by comparing the actual motion response of the vehicle with the simulated response from a calm water based mathematical model. In addition, AUV simulators are used by vehicle developers and operators to test their mission plans and software modifications as well as to conduct trainings prior to field trials [16]. Such simulators need a mathematical model with precise representation of the vehicle characteristics to accurately simulate the dynamic motion response of the AUV.

The hydrodynamic forces acting on AUVs are highly nonlinear; hence, mathematical models should contain higher-order hydrodynamic coefficients to represent these nonlinear characteristics. Previous works have introduced a number of methods to determine linear and nonlinear hydrodynamic coefficients of marine vehicles including the coupling effects between different motion modes; for example, captive model experiments [13,17], computational fluid dynamics (CFD) simulation methods [13,18] and system identification using field data [15,19,20]. Some of these efforts also account for environmental and external forces; although for underwater vehicles, these forces are generally based on wave and wind histogram data of a particular location [21]. However, previous data do not precisely reflect local variations of environmental condition and hence may not replicate true external forces.

This paper presents a system identification algorithm to determine the linear and nonlinear parameters of an AUV mathematical model utilising the recursive least squares (RLS) and the prediction error method (PEM) optimisation techniques. The developed model accounts for the coupling effects influencing the surge, sway and heave velocities of the vehicle as well as the environmental and external forces. Utilising the model

Fig. 1 Body-fixed frame of reference and the configuration of the utilised *Gavia* AUV. The origin is located at the centre of buoyancy of the vehicle. The vehicle had a length of 2.7 m, a diameter of 0.2 m, and a dry weight in air of approximately 70 kg
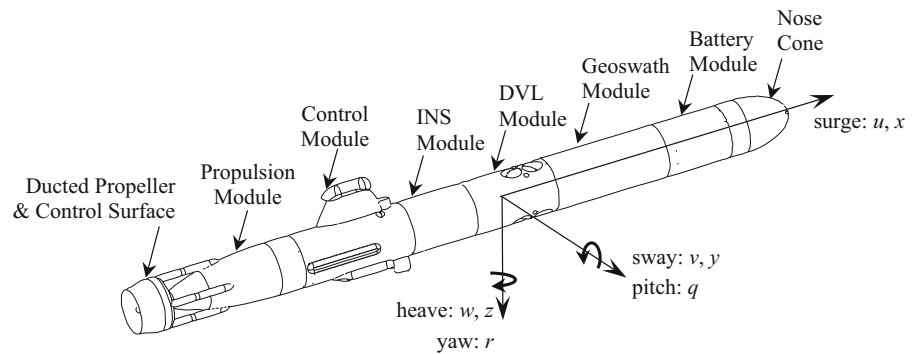
identification algorithms, the parameters of a *Gavia* class AUV mathematical model were estimated using motion response data from a complex identification manoeuvre conducted in a small, relatively calm lake (i.e. minimal surface mixing. A comparison is made between RLS and PEM, and the dependency of the parameters on the utilised dataset is also investigated. The identified model parameters are able to predict the motion response of the AUV in calm water condition and are referred to as the 'baseline' mathematical model hereafter. A novel technique is presented to field calibrate the baseline mathematical model to predict the vehicle motion response in diverse operational environments. The model calibration algorithm was extended to determine the AUV mathematical model in real time, processing a limited preceding data window for future goals such as real-time control system optimisation. The following sections of this paper provide an overview of the field experimental setup (including the details of the utilised *Gavia* AUV and test site details), theory and justification of AUV dynamic modelling equations utilised in this study, and a brief description of the RLS and PEM techniques and the model simulation method. Baseline model estimation procedure and model calibration method are then explained together with a performance analysis. Finally, the real-time model calibration is discussed, followed by a summary on possible future developments and conclusions.

2 Field experimental setup

2.1 Instrumentation

The system parameter identification algorithm was developed for a *Gavia*-class modular AUV [22] using the vehicle motion response data collected during various field trials. Due to the modularity of the vehicle,

the component arrangement can be changed, which will alter the hydrostatic and hydrodynamic characteristics of the vehicle on any given deployment. The vehicle in the tested configuration (see Fig. 1) consisted of a Nose Cone Module, Battery Module, Geoswath Interferometric Sonar Module, 1200 kHz Teledyne RDI Acoustic Doppler Current Profiler (ADCP) / DVL Module, Kearfott T24 INS (KI-4902S model) Module, Control Module, and a Propulsion Module. The vehicle had a length of 2.7 m, a diameter of 0.2 m, and a dry weight in air of approximately 70 kg. The propulsion module was a three-bladed ducted propeller system with four individually functioning control surfaces arranged in an 'X' configuration.

The DVL-aided Kearfott T24 INS measured the accelerations in six-degree-of-freedom (6-DOF) and orientation, to make estimates of the AUV's velocities and position. The heading and pitch angles of the vehicle were measured by the gyroscopic sensors, while the accelerations were determined through the use of accelerometers within the INS unit. The vehicle position estimate was corrected with the velocities over ground from the bottom tracking DVL (i.e. when the altitude of the AUV is below the range of the DVL acoustic beams) in order to avoid drifts in the derived localisation solution. The depth of the vehicle was obtained from the Keller Series 33Xe pressure sensor on-board the AUV. All sensor measurements were sampled at a frequency of 0.87 Hz and recorded in the vehicle log. The uncertainties of these instruments and the other sensors associated with the navigation unit are outlined in Table 1.

2.2 Test site and experimental runs

The objectives of the field studies were to develop and to validate the parameter identification and cal-

Table 1 Specifications of *Gavia* AUV sensor packages. CEP for circular error probable and TRMS for time mean root squared

Sensor package	Measurements	Measurement accuracy
DVL-bottom-track/GPS-aided INS	Heading angle	$\pm\,0.010°$ (RMS)
	Pitch angle	$\pm\,0.005°$ (RMS)
	Position estimate	0.1% of the distance travelled (CEP)
	Velocity estimate (DVL aided)	$0.001\,\mathrm{m\,s^{-1}}$ (RMS)
	Velocity estimate (GPS aided)	$0.05\,\mathrm{m\,s^{-1}}$ (RMS)
DVL-water-track-aided INS	Position estimate	1852 m per 8 h (TRMS)
		4.02% of the distance travelled[a]
	Velocity estimate	$0.3\,\mathrm{m\,s^{-1}}$ (RMS)
1200 kHz Teledyne RDI DVL	Bottom tracking AUV velocity	$\pm\,0.001\,\mathrm{m\,s^{-1}}$ (RMS) or 0.2% of the velocity
	Maximum bottom tracking range	30 m
Keller Series 33Xe pressure sensor	Vehicle depth	0.1% of the depth

[a]Derived from the 1 nm per 8 h uncertainty value for comparison, assuming an AUV forward speed of $1.6\,\mathrm{m\,s^{-1}}$

ibration algorithms for different environments. Field studies were conducted in two locations: Lake Trevallyn in Tasmania, Australia (Fig. 2a), and in Lake Ohau, South Island, New Zealand (Fig. 2b).

During the Lake Trevallyn missions, the surface wave heights were less than 50 mm and the vehicle's ADCP recorded minor variations of the water column velocities, with averaged values of surge, sway and heave directions of 0.002, 0.002 and $0.001\,\mathrm{m\,s^{-1}}$, respectively. Due to these very small flow velocities, Lake Trevallyn can be classified as a calm water environment.

The Lake Ohau test site, on the other hand, reveals a more dynamic flow conditions due to its size and exposure to stronger external forces. The surface wave heights at time of conducting operations were around 0.3 m, and the magnitudes of near surface water currents close to the inflow points of the Hopkins and Dobson Rivers measured from the vehicle ADCP were around $0.15\,\mathrm{m\,s^{-1}}$ [23]. The test site at Lake Ohau had highly variable bathymetry, i.e. rough in proximity of the delta front as well as relatively flat lake floor in deeper parts of the lake (Fig. 2c). For constant altitude AUV missions, the vehicle experienced highly fluctuating pitch angles (i.e. over $\pm\,10°$) when flying above the region of variable bathymetry (i.e. up to 200 m from the starting position), while angles of less than $\pm\,2°$ were maintained above the flat terrain. For these reasons, the test site was decided to be a suitable stage to test the AUV mathematical models for different vehicle responses.

Lake Trevallyn field data were used to identify the baseline parameters of the mathematical model due to the lake's calm water condition with no external forcings. Two identification manoeuvres, named ID Manoeuvre 1 and ID Manoeuvre 2, were conducted to investigate the variation of the parameters on the utilised dataset. In order to successfully identify the model parameters, each manoeuvre consisted of three types of runs that stimulate the six motion modes (i.e. surge, sway, heave, roll, pitch and yaw). For example, in ID Manoeuvre 1, the AUV performed zig-zag runs in yaw (from 0 to 260 s as in Fig. 3) and pitch (from 260 to 660 s as in Fig. 3) planes by changing the coordinate way points and operating depths concurrently. From 660 to 900 s, the propeller speed was increased in steps from 450 to 975 RPM, covering the typical operational RPM range of the *Gavia* AUV. The pitch angle of the AUV unintentionally fluctuated, while the horizontal heading angle was changed (Fig. 3). Similarly, the horizontal heading oscillated, while the depth changes were executed, stimulating coupling effects between the motion modes. Such unintentional fluctuations in pitch and yaw were low during the straight line runs. The propeller speed was varied to maintain a constant speed during the heading zig-zag runs. Water depths in Lake Trevallyn vary between 10 and 15 m and the AUV missions were carried out between 2 and 8 m below the free surface to minimise the bias due to surface wave formation [24] and interaction with the lake bottom [12]. Similarly, ID Manoeuvre 2 consisted of zig-zag runs in both pitch and yaw planes, and runs

Fig. 2 AUV field deployments were conducted **a** in Lake Trevallyn, Tasmania, Australia, and **b** Lake Ohau, South Island, New Zealand. Parameters of the mathematical model were determined from the manoeuvres conducted in Lake Trevallyn. The estimated models were verified with the vehicle motion response data from AUV deployments in Lake Ohau—eight AUV runs were conducted in a lawn-mover pattern (inset). **c** Bathymetry along the AUV track line (1) conducted in Lake Ohau, New Zealand
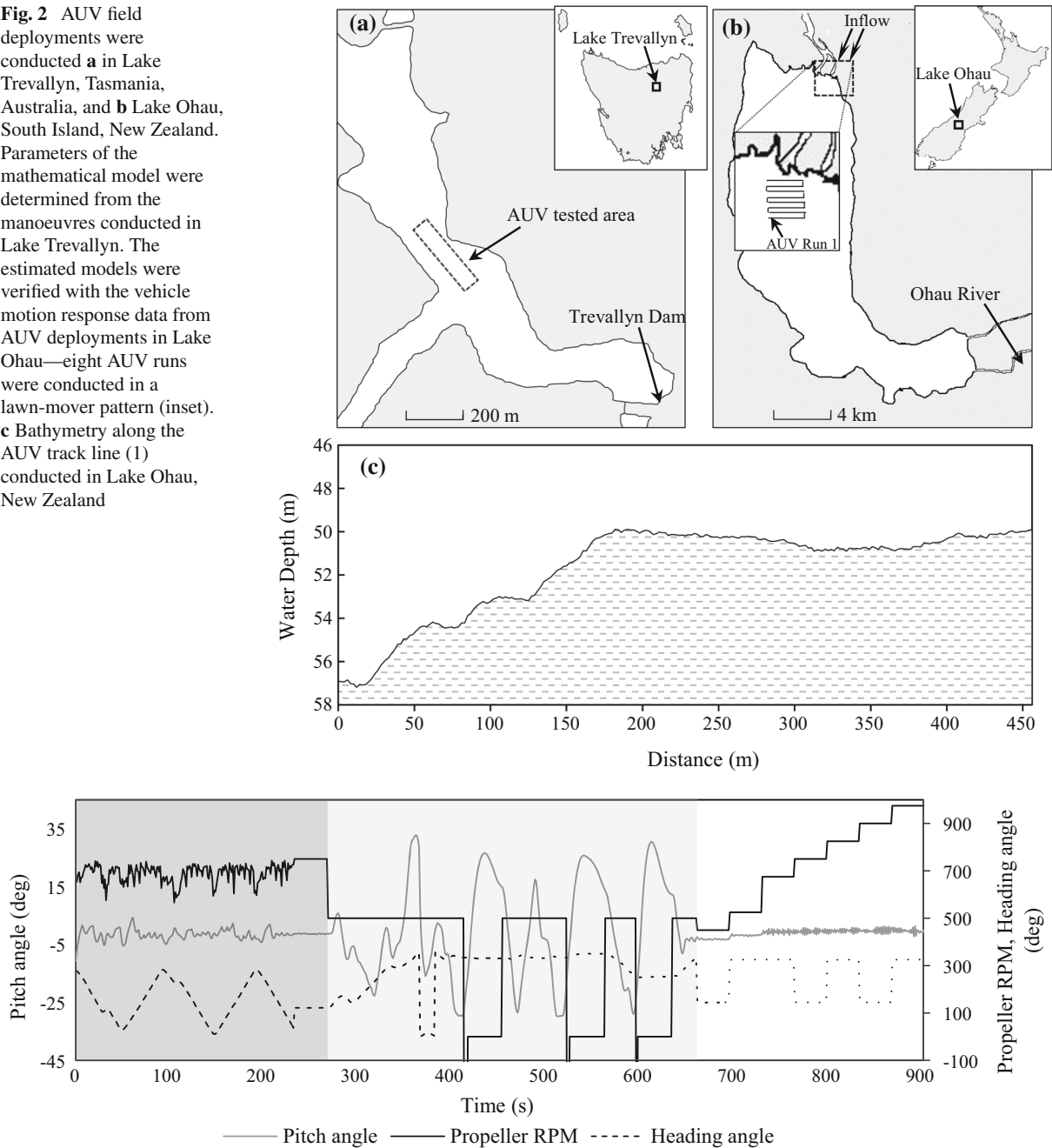

Fig. 3 The AUV motion response during a sample identification manoeuvre (i.e. ID Manoeuvre 1) conducted in Lake Trevallyn site. The manoeuvre consisted of three types of runs that stimulate the six motion modes, i.e. zig-zag manoeuvres in yaw plane (section shaded in dark grey) and pitch plane (shaded in light grey), and step changes of propeller speed from 450 to 975 RPM (no shading)

with different propeller speeds. The ID Manoeuvre 2 was carried out 6–12 m below the free surface.

In Lake Ohau, a lawn-mower pattern mission with eight transect lines was conducted. Each straight line run was carried out over the diverse bathymetry (i.e. the water depth was varying from around 50–60 m) maintaining a constant altitude of 8 m above the seabed. The first four lines (runs 1–4) of the lawn-mower pattern were used to calibrate the baseline model for the Lake Ohau water column condition utilising the model calibration method introduced in this work. The performance improvement of the calibrated model compared to the baseline model was analysed by testing the model with the last four lines (runs 5–8). Therefore, both calibration and performance analysis runs included smooth as well as rough bathymetric conditions.

Validation of the real-time model estimation algorithm was conducted in Trevallyn as well as Ohau sites in order to establish its robustness in different field conditions. During all field tests, the vehicle altitude was within the range of the DVL acoustic beams, continuously aiding the INS solution. Hence, the motion response measurements used for model validations were maintained within the DVL-aided INS uncertainty limits as given in Table 1.

3 Dynamic modelling of the AUV

Manoeuvring equations of motion derived by considering the rigid-body kinetics, hydrodynamics, hydrostatics, environmental and other external forces acting on the AUV are generally used for vehicle modelling [21,25,26]. In the work presented here, we used a basic mathematical model given in Eq. (1) as specified for underwater vehicles by Fossen [26]; however, the hydrodynamic, environmental and control forces were modelled using a new mathematical model. One of the key advantages of this work is that the utilised mathematical model can be applied for any torpedo-shaped AUV of any configuration. The mathematical formulae presented in this paper are based on the SNAME (1952) notation, with the associated coordinate system shown in Fig. 1.

$$\mathbf{M_{RB}}\dot{\vec{v}} + \mathbf{C_{RB}}\left(\vec{v}\right)\vec{v} + \mathbf{M_A}\dot{\vec{v}} + \mathbf{C_A}\left(\vec{v}\right)\vec{v}$$
$$+ \mathbf{D}\left(\vec{v}\right)\vec{v} + \mathbf{g}\left(\eta\right) = \tau + \tau_{\mathbf{external}} \tag{1}$$

where $\mathbf{M_{RB}}$ and $\mathbf{M_A}$ are the rigid body and added mass system inertia matrices, $\mathbf{C_{RB}}$ and $\mathbf{C_A}$ are the

rigid body and added mass Coriolis–centripetal matrices, $\mathbf{D}$ is the hydrodynamic damping matrix, $\mathbf{g}\left(\eta\right)$ is the restoring gravitational/buoyancy force matrix, τ is the vector of propulsion and control surface forces, and τ_{external} represents the vector of environmental and external forces. The vector $\vec{v}$ denotes the velocity (i.e. $[u, v, w, p, q, r]^{\mathrm{T}}$ where u, v, w and p, q, r are the linear and angular velocities around the x, y and z axes), and η is the vector of position/Euler angles (i.e. $\eta = [x, y, z, \varphi, \theta, \psi]$ where φ, θ and ψ are the roll, pitch and yaw angles, respectively) as illustrated in Fig. 1.

3.1 System inertia, Coriolis–centripetal and hydrostatic forces

Using the approach of Fossen [26], Eqs. (2), (3) and (4) present the mathematical models in x, y and z directions of the AUV, respectively. The left-hand sides of these equations represent the inertia, Coriolis–centripetal and hydrostatic force components along each direction. Inertial and Coriolis–centripetal forces contain both mass and added mass components that have a vital contribution in marine vehicle dynamics.

$$(m - X_{\dot{u}})\,\dot{u} + mz_g\dot{q} - my_g\dot{r} - (W - B)\sin(\theta)$$
$$- X_{\text{prop}} = \sum \mathbf{X} \tag{2}$$

$$(m - Y_{\dot{v}})\,\dot{v} - mz_g\dot{p} + \left(mx_g - Y_{\dot{r}}\right)\dot{r} = \sum \mathbf{Y} \tag{3}$$

$$(m - Z_{\dot{w}})\,\dot{w} - \left(mx_g - Z_{\dot{q}}\right)\dot{q} - (W - B) = \sum \mathbf{Z} \tag{4}$$

where the term m is the mass of the vehicle and x_g, y_g and z_g represent the position of the centre of gravity in x, y and z directions, respectively, from the centre of buoyancy of the vehicle. Further, W is the weight of the vehicle in air, B is the buoyancy force, θ is the pitch angle, and X_{prop} is the thrust produced by the propeller. The right-hand side of these equations (i.e. $\sum \mathbf{X}, \sum \mathbf{Y}$ and $\sum \mathbf{Z}$) represents the summation of hydrodynamic damping, and environmental and external forces.

3.2 Hydrodynamic damping and external and environmental forces

Hydrodynamic damping of underwater vehicles is a result of several factors including (1) the linear skin friction due to laminar boundary layer dynamics, (2) the

nonlinear skin friction due to turbulent boundary layer dynamics, (3) the viscous damping force due to vortex shedding, (4) the form drag due to pressure variation across the body, and (5) the hydrodynamic lift forces due to cross-flow drag and circulation of water around the hull [21]. Therefore, linear as well as higher-order damping terms and relevant cross-flow coupling terms are required to accurately model the flow around the vehicle [21,27]. It is also important to model the vehicle dynamics with a minimum number of parameters because if the number of unknown parameters present in a model is large, the accuracy of the parameter estimation reduces [28].

When using a mathematical model, an accurate description of environmental and external forces is required for calibration. In marine vehicle modelling, it is common to assume the principle of superposition when considering these highly nonlinear forces [21]. This principle suggests that the generalised environmental and external forces are added to the right-hand side of Eq. (1); i.e. τ_{external}.

3.2.1 Forces in x direction

In the current work, the hydrodynamic damping along the x direction is modelled using Eq. (5).

$$\sum \mathbf{X} = X_{uuu}u^3 + X_{u|u|}u\,|u| + X_u u + X_{wq}wq \\ + X_{vr}vr + X_{\psi|\psi|}\psi\,|\psi| + X_\psi\psi + X_{\text{static}} \tag{5}$$

where the notation of the hydrodynamic coefficients follow SNAME (1952). For example, X_u is the derivative of the surge force (X) with respect to the surge speed (u), i.e. $X_u = \partial X/\partial u$. $X_{\psi|\psi|}$ and X_ψ are the surge force coefficients due to underwater currents. X_{static} stands for variable independent static external forces along x direction.

This equation is comprised of damping terms up to the third order (i.e. X_u, $X_{u|u|}$ and X_{uuu}); hence, it includes laminar and turbulent skin friction damping components as well as viscous damping. The terms X_{wq} and X_{vr} represent the cross-coupled drag components, i.e. change in the forward speed of the AUV resulting from heading and pitch variations. The external forces due to underwater currents depend on the heading of the vehicle. For example, if a steady underwater current is flowing from North to South, the external current force component acting on the vehicle when

travelling with a heading angle of 0° would be different to a heading angle of 60°. Fossen [21] models the forces due to underwater currents as a function of angle of attack of the AUV with the flow direction, which is also a function of the vehicle heading angle. Hence, in this work, external forces along the x direction due to current are modelled as functions of up to the second order of the vehicle heading (i.e. $X_{\psi|\psi|}$ and X_ψ). Other environmental and external forces (i.e. direction independent) acting along the x direction are assumed to be superimposed within the damping hydrodynamic parameters. This offers the ability to capture the external forces as functions of all the previously stated variables, maximising the accuracy of model calibration for different environmental conditions. However, this has a disadvantage of not being able to obtain values for the pure hydrodynamic derivatives as environmental and external forces are incorporated in them. Any uncaptured steady external forces are included in the model as a variable independent constant X_{static}.

3.2.2 Forces in y direction

Similarly, the hydrodynamic damping forces and environmental/external forces acting along the y direction are modelled using Eq. (6).

$$\sum \mathbf{Y} = Y_{v|v|}v\,|v| + Y_v v + Y_q q + Y_r r + Y_p p \\ + Y_{\psi|\psi|}\psi\,|\psi| + Y_\psi\psi + Y_{\text{static}} \tag{6}$$

Nonlinear hydrodynamic damping along y direction was limited to the second order of the sway velocity (i.e. Y_v and $Y_{v|v|}$). The *Gavia* AUV is asymmetric about the x–y and y–z—planes. Therefore, as the vehicle presents an angle of yaw to the flow (i.e. as the vehicle changes its horizontal heading angle), the AUV will start to roll and pitch, resulting in a change in the vehicle operating depth as the control system responds. Due to the asymmetry of the vehicle, this will occur in all directions. Therefore, the linear cross-coupled drag components due to roll, pitch and yaw motions (i.e. Y_p, Y_q and Y_r) were also included in Eq. (6). Similar to the surge model, the sway force due to steady underwater currents is modelled as functions of up to the second order of the vehicle heading (i.e. $Y_{\psi|\psi|}$ and Y_ψ). The direction-independent environmental/external forces acting along the sway direction are assumed to be superimposed within the hydrodynamic damping terms. Uncaptured steady external

forces are incorporated as a variable independent constant Y_{static}.

3.2.3 Forces in z direction

Equation (7) describes the hydrodynamic damping and environmental/external force along the heave direction.

$$\sum \mathbf{Z} = Z_{w|w|} w \, |w| + Z_w w + Z_q q + Z_r r + Z_{\text{static}}$$
(7)

Similar to the sway force component, the nonlinear hydrodynamic damping in the z direction was limited to the second order of the heave velocity (i.e. Z_w and $Z_{w|w|}$). The cross-coupled damping terms due to pitch and yaw motions (i.e. Z_q and Z_r) were also included. The environmental/external forces acting along the heave direction were also assumed to be superimposed within the modelled hydrodynamic damping parameters. Uncaptured steady external forces are incorporated as a variable independent constant Z_{static}, which also represents any variations in the ballast condition from the baseline model. The heading direction-dependent underwater currents along the vertical direction are neglected.

3.3 Final dynamic equations of motion and control forces

Equations (2) and (5) are combined and rearranged to determine the surge acceleration as shown in Eq. (8).

$$\dot{u} = \frac{1}{(m - X_{\dot{u}})} [m y_g \dot{r} - m z_g \dot{q} + (W - B) \sin (\theta)$$
$$+ X_{uuu} u^3 + X_{u|u|} u \, |u| + X_u u + X_{wq} wq$$
$$+ X_{vr} vr + X_{\psi|\psi|} \psi |\psi| + X_\psi \psi$$
$$+ X_{\text{static}} + X_{\text{prop}}]$$
(8)

where X_{prop} is the thrust produced by the propeller that is given by $X_n \times RPM^2$. RPM is the vehicle's propeller revolutions per minute and X_n is the thrust coefficient, which is 95×10^{-6} for the *Gavia* AUV according to the estimation by Þorgilsson [22]. The thrust coefficient is only valid for the propeller speed range from 450 to 975 RPM.

The mass, added mass, buoyancy and the positions of the centre of gravity of the AUV vary with the vehicle configuration and the ballast condition. Therefore, these values are deployment dependent. Equation (8) is

parameterised as shown in Eq. (9) in order to superimpose these unknown properties inside the parameters to be identified, eliminating the requirement to measure those physical properties of the AUV. However, this has a disadvantage of not being able to obtain values for the pure hydrodynamic derivatives as other properties are overlaid within them.

$$\dot{u} - X_n \times \text{RPM}^2 = \alpha_1 \dot{r} + \alpha_2 \dot{q} + \alpha_3 \sin (\theta) + \alpha_4 u^3$$
$$+ \alpha_5 u \, |u| + \alpha_6 u + \alpha_7 wq + \alpha_8 vr$$
$$+ \alpha_9 \psi |\psi| + \alpha_{10} \psi + \alpha_{11}$$
(9)

where $\alpha_1, \alpha_2 \ldots \alpha_{11}$ are the parameters to be estimated using the identification algorithm.

Similarly, Eqs. (3) and (6), and Eqs. (4) and (7) are combined, rearranged, and parameterised as shown in Eqs. (10) and (11), respectively.

$$\dot{v} = \beta_1 \dot{r} + \beta_2 \dot{p} + \beta_3 v \, |v| + \beta_4 v + \beta_5 p + \beta_6 q$$
$$+ \beta_7 r + \beta_8 \psi |\psi| + \beta_9 \psi + \beta_{10}$$
(10)

$$\dot{w} = \gamma_1 \dot{q} + \gamma_2 w \, |w| + \gamma_3 w + \gamma_4 q + \gamma_5 r + \gamma_6$$
(11)

where $\beta_1, \beta_2 \ldots \beta_{10}$ and $\gamma_1, \gamma_2 \ldots \gamma_6$ are the parameters to be estimated using the identification algorithm developed in this work.

Roll, pitch and heading angles of an AUV could be measured using the gyroscopic sensors inside the vehicle INS regardless of the availability of external velocity aiding from DVL. For this reason, it was determined that estimating Euler angles of the AUV were not required for this work. Hence, roll, pitch and yaw angular velocities and accelerations (i.e. p, q, r, $\dot{p}, \dot{q}$ and $\dot{r}$) were directly provided as inputs into the model. This provided the ability to limit the mathematical model to 3-DOF (i.e. linear motions along x, y and z directions), eliminating the requirement to model the rolling, pitching and yawing motions. This also had the added advantage of the actuator control surfaces in Eqs. (9), (10) and (11) not having to be modelled. Instead the actual turning behaviours of the vehicle (i.e. p, q, r, $\dot{p}, \dot{q}$ and $\dot{r}$) measured during the tests were provided as model inputs. The propulsion module utilised for this work had four independently operating control surfaces in a 'X' configuration. This arrangement concurrently generates moments around both y and z directions, incorporating complicated coupling effects between the control surfaces [29]. As a result of the 3-DOF modelling used in this work, resolving the produced moments were not necessary.

4 Parameter identification and simulation model

4.1 Recursive least squares (RLS) identification

Recursive least squares-based parameter identification was conducted using the recursive least squares estimation block set of MATLAB's System Identification toolbox, which is based on the theoretical approach outlined in Ljung [28]. Equations (9), (10) and (11) are modified to the format given in Eq. (12).

$$\mathbf{y}_{(t)} = \mathbf{H}_{(t)}\mathbf{\Theta}_{(t)} \tag{12}$$

where $\mathbf{y}_{(t)}, \mathbf{H}_{(t)}$ and $\mathbf{\Theta}_{(t)}$ are vectors as defined in Table 2 for surge, sway and heave models.

In the standard Least Squares Estimation method, the entire data set is processed concurrently to determine the parameter vectors; i.e. $\mathbf{\Theta}_{(t)}$ in Eq. (12), by solving Eq. (13).

$$\mathbf{\Theta}_{(t)} = \left[\mathbf{H}_{(t)}^T\mathbf{H}_{(t)}\right]^{-1}\mathbf{H}_{(t)}^T\mathbf{y}_{(t)} \tag{13}$$

While the AUV is under operation, new motion response data are continuously being measured and sampled at each time step. If the standard Least Squares Estimation method is employed, it requires the identification algorithm to be rerun for the entire mission (i.e. for all the data from the initial time step to the current time step) with the arrival of each new measurement [28]. On the other hand, the RLS estimation method adds the subsequent measurements to the existing solution without requiring the algorithm to be rerun. Equation (14) shows how the estimated parameters are extended for the subsequent measurements [28].

$$\mathbf{\Theta}_{(t)} = \mathbf{\Theta}_{(t-1)} + \mathbf{P}_{(t)}\mathbf{H}_{(t-1)}\boldsymbol{\varepsilon}_{(t)} \tag{14}$$

where t is the time step and,

$$\boldsymbol{\varepsilon}_{(t)} = \mathbf{y}_{(t)} - \mathbf{H}_{(t)}\mathbf{\Theta}_{(t-1)},$$

$$\mathbf{P}_{(t)} = \frac{\tilde{\mathbf{P}}_{(t)}}{\lambda}$$

$$\tilde{\mathbf{P}}_{(t)} = \mathbf{P}_{(t-1)} - \frac{\mathbf{P}_{(t-1)}\mathbf{H}_{(t-1)}\mathbf{H}_{(t-1)}^T\mathbf{P}_{(t-1)}}{\lambda + \mathbf{H}_{(t-1)}^{\mathrm{T}}\mathbf{P}_{(t-1)}\mathbf{H}_{(t-1)}}$$

and where λ is the forgetting factor.

$$\lambda = 1 - \frac{1}{T_0}$$

where T_0 is the length of the preceding data set that will be processed during the identification process. Thus, past measurement data can be removed with the arrival of new data, and therefore, successive measurements can have a higher weight in the estimation process. The maximum value of the forgetting factor is one, which corresponds to none of the past data being forgotten (i.e. the entire dataset from the beginning to the current time step will have an equal weight). The smaller the forgetting factor, the shorter the length of the utilised preceding data set. This is important when the variation of parameters has to be identified in real time in dynamic operational environments with varying environmental and external forcing.

The initial values of all the parameters were set to 1 in order to retain the assumption that the initial parameters of the AUV model are unknown to the user.

4.2 Prediction error method (PEM) identification

Prediction error estimation function of MATLAB System Identification toolbox was utilised for PEM-based parameter identification. PEM identification is done by minimising the difference between the predicted outputs $\hat{\mathbf{y}}(t)$ (i.e. the outputs of Eqs. (9), (10) and (11) according to parameters $\mathbf{\Theta}_{(t)}$ that is being estimated recursively) and measured outputs $\mathbf{y}_{(t)}$ as given in Table 2.

$$\mathbf{\Theta}_{(t)} = \underset{\mathbf{\Theta}}{\arg\min}\, V\left(\mathbf{\Theta}_{(t)}\right) \tag{15}$$

Table 2 $\mathbf{y}_{(t)}, \mathbf{H}_{(t)}$ and $\mathbf{\Theta}_{(t)}$ vectors of Eqs. (12) and (16) for x, y and z directions

x direction $\mathbf{y}_{(t)} = \dot{u} - X_n \times RPM^2$	y direction $\mathbf{y}_{(t)} = \dot{v}$	z direction $\mathbf{y}_{(t)} = \dot{w}$
$\mathbf{H}_{(t)} = \begin{bmatrix} \dot{r} & \dot{q} & \sin(\theta) & u^3 \\ u\,\vert u\vert & u & wq & vr & \phi^2 & \phi & 1 \end{bmatrix}$	$\mathbf{H}_{(t)} = \begin{bmatrix} \dot{r} & \dot{p} & v\,\vert v\vert & v \\ p & q & r & \phi^2 & \phi & 1 \end{bmatrix}$	$\mathbf{H}_{(t)} = \begin{bmatrix} \dot{q} & 1 & w\,\vert w\vert & w & q & r \end{bmatrix}$
$\Theta_{(t)} = \begin{bmatrix} \alpha_1 & \alpha_2 & \alpha_3 & \alpha_4 & \alpha_5 \\ \alpha_6 & \alpha_7 & \alpha_8 & \alpha_9 & \alpha_{10} & \alpha_{11} \end{bmatrix}$	$\mathbf{\Theta}_{(t)} = \begin{bmatrix} \beta_1 & \beta_2 & \beta_3 & \beta_4 \\ \beta_5 & \beta_6 & \beta_7 & \beta_8 & \beta_9 & \beta_{10} \end{bmatrix}$	$\mathbf{\Theta}_{(t)} = \begin{bmatrix} \gamma_1 & \gamma_2 & \gamma_3 & \gamma_4 & \gamma_5 & \gamma_6 \end{bmatrix}$

where,

$$V\left(\mathbf{\Theta}_{(t)}\right) = \frac{1}{2N} \sum_{t=1}^{N} \left\| y_{(t)} - \hat{y}_{t|t-1(\mathbf{\Theta}_{(t-1)})} \right\|^2$$

where $\hat{y}_{t|t-1(\mathbf{\Theta}_{(t-1)})}$ is the predicted linear acceleration output at t, using all the information until time $t-1$.

Similar to the RLS estimation, the initial values of all the parameters were set to 1. The computation of the minimising argument is a complicated process with a substantial amount of calculations. A thorough discussion regarding this process is given in Ljung [28].

4.3 Simulation model

The simulation model described in this section can be used to determine u, v, and w once the parameters (i.e. $\mathbf{\Theta}_{(t)}$) are completely estimated or the estimation is being carried out in real time. The acceleration vectors of the current time step in the x, y and z directions are calculated according to Eqs. (9), (10) and (11), respectively, using the controlling commands (i.e. the time stamps of propeller RPM, roll rate, roll acceleration, pitch rate, pitch acceleration, yaw rate and yaw acceleration) of the vehicle and the velocity vector from the previous time step (Fig. 4). For real-time conditions, the parameter vector will be updated at each time step, while for non-real-time applications, it will remain constant. The calculated acceleration vector is then integrated with respect to the time in order to obtain the velocity vector (i.e. u, v and w) in the body-fixed reference frame. This process is repeated with a time step of 0.0001s for the entire mission time. The selected time step is large enough to maintain a low computational time and small enough to converge the velocity solu-

tion between two control command sampling intervals (i.e. of 0.87 Hz).

5 Baseline model identification and calibration

The primary application of mathematical model identification is to determine the unknown parameters of the AUV mathematical model in order to estimate the surge, sway and heave velocities of the vehicle when DVL velocity measurements are unavailable.

5.1 Baseline model identification

Baseline mathematical models that represent the dynamics of the *Gavia* AUV in a calm water environment were first determined using the RLS and PEM system identification algorithms. Since external and environmental forces caused by currents, turbidity, pressure fluctuations, etc., are neglected in the baseline model, the surge and sway force parameters due to steady underwater currents (i.e. α_9, α_{10}, β_8 and β_9) and uncaptured steady external forces (i.e. α_{11} and β_{10}) were removed from Eqs. (9) and (10). However, minor external/environmental forces might be incorporated within the remaining parameters of the model. The parameter representing the steady external forces along z direction (i.e. γ_6) was not removed from Eq. (11) as it also represents the $(B - W)$ term as shown in Eq. (4). For the RLS method, a forgetting factor of one was utilised in order to process the entire length of the data set with an equal weight (i.e. no forgetting) and determine the parameter vectors (i.e. $\mathbf{\Theta}_{(t)}$) by solving Eqs. (13) and (14). To establish baseline conditions, the identification

Fig. 4 Simulation model flowchart. The solution for the acceleration vector of the current time step is determined using the control command vectors and velocity vectors from the previous time step. The velocity vector is then calculated by integrating the acceleration vector with respect to time. *The parameter vector remains constant for non-real-time identification
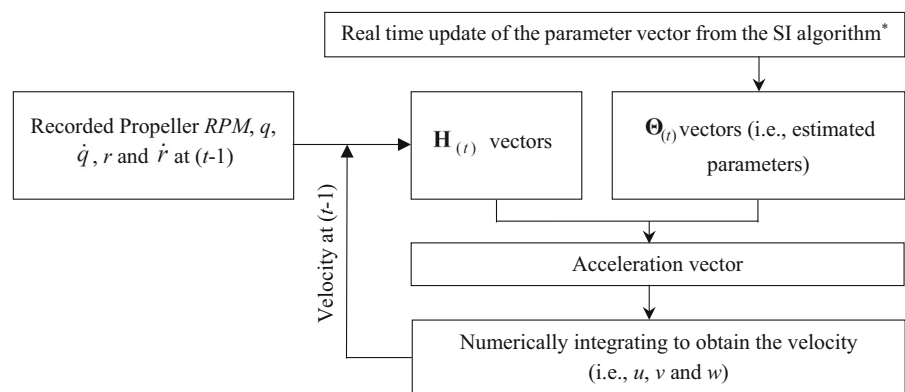
algorithm was run using Lake Trevallyn field manoeuvres (i.e. ID Manoeuvres 1 and 2).

Parameter identification was conducted with both RLS and PEM techniques to determine the most effective estimation method for the mathematical model defined in this work. In order to investigate parameter estimation using a dataset with dissimilar inputs and outputs, each identification technique (i.e. RLS and PEM) was repeated for the two identification manoeuvres (i.e. for ID Manoeuvres 1 and 2). At the end of each identification process, parameter values had converged within 5% of the mean values. These baseline parameters for the vehicle (as configured) are presented in Table 3.

5.2 Model calibration

The baseline mathematical model may be unable to predict the vehicle motion response in operational environments different from the baseline environment. For example, if the vehicle is operating in a highly turbulent waters, the baseline model will be unable to predict the AUV's actual velocities over ground. Similarly, variations in the vehicle setting due to different ballast and trim conditions, addition of new payloads, and change in module configuration will change the hydrostatic and hydrodynamic forces acting on the AUV and hence, the mathematical model representing it. Therefore, any deviation from the baseline vehicle condition requires alteration of the mathematical model to obtain an accurate motion response. A model calibrating algorithm was introduced to overcome this by adjusting the baseline model for the new vehicle operational environments and configurations by carrying out a calibration mission.

For model calibration, the RLS algorithm was run for Eq. (16) instead of for Eq. (12). That is, in Eq. (16), $\mathbf{y}_{(t)}$ and $\mathbf{\Theta}_{(t)}$ of Eq. (13) will be replaced by the terms $(\mathbf{y}_{(t)} - \mathbf{F})$ and $\mathbf{\Theta}_{(t),\mathrm{alteration}}$, respectively.

$$\mathbf{y}_{(t)} - \mathbf{F} = \mathbf{H}_{(t)}\mathbf{\Theta}_{(t),\mathrm{alteration}} \qquad (16)$$

where $\mathbf{y}_{(t)}$ and $\mathbf{H}_{(t)}$ are as defined in Table 2 for surge, sway and heave models, while $\mathbf{F}$ reflects the right-hand side in Eqs. (9), (10) and (11), respectively. The baseline model was used to obtain the solutions for $\mathbf{F}$. The terms in $\mathbf{\Theta}_{(t),\mathrm{alteration}}$ represent the corrections required for the initial parameters in the baseline model.

In this investigation, the baseline model identified with the RLS method using ID Manoeuvre 1 was calibrated to predict the vehicle motion response in the environmental conditions in Lake Ohau. The same *Gavia* AUV with the identical module configuration as in the Lake Trevallyn tests was used for Lake Ohau mission. Therefore, the mass and hydrostatic vehicle properties were unaffected, and the corresponding parameters were not calibrated. Thus, α_1, α_2, α_3, β_1, β_2 and γ_1 parameters and corresponding motion variable elements were removed from $\mathbf{\Theta}_{(t),\mathrm{alteration}}$ and $\mathbf{H}_{(t)}$ vector, respectively. Surge and sway force parameters due to steady underwater currents (i.e. α_9, α_{10}, β_8 and β_9) and external forces (i.e. α_{11} and β_{10}), which were neglected in the baseline model, were included for the model calibration as the objective is to capture the effect of environmental forces. At the end of the calibration run, the calibrated parameters were obtained by adding the required corrections to the original baseline parameters according to Eq. (17).

$$\mathbf{\Theta}_{(t),\mathrm{calibrated}} = \mathbf{\Theta}_{(t)} + \mathbf{\Theta}_{(t),\mathrm{alteration}} \qquad (17)$$

where $\mathbf{\Theta}_{(t),\mathrm{calibrated}}$ is the final set of calibrated parameters.

5.3 Performance analysis and discussion

Performances of the determined baseline models were examined by applying the identified parameter vectors (i.e. $\mathbf{\Theta}_{(t)}$) into the simulation model and simulating a set of pitch and yaw plane zig-zag manoeuvres conducted in Lake Trevallyn (i.e. under the same environmental and vehicle conditions). The AUV runs used for model estimations were not used for this validation process to have an unbiased validation.

Simulated vehicle velocities from baseline models were compared against actual measurements from the DVL-aided INS. Baseline models included those identified using RLS and PEM techniques, with each technique processed twice using field data from ID Manoeuvres 1 and 2. Figure 5a–c compares the experimental and model predicted velocities in surge, sway and heave directions, respectively (i.e. u, v and w). The uncertainties in surge velocity predictions from all models increase with time due to accumulation of acceleration prediction error during the integration to determine the velocity. Conversely, the error propa-

Table 3 Numerical values of the *Gavia* AUV's baseline parameters determined from RLS and PEM techniques using ID Manoeuvres 1 and 2

Parameter	RLS (ID Manoeuvre 1)	RLS (ID Manoeuvre 2)	PEM (ID Manoeuvre 1)	PEM (ID Manoeuvre 2)
$\alpha_1 = \frac{m y_g}{(m - X_{\dot{u}})}$	0.5294	0.3502	0.5279	0.4448
$\alpha_2 = \frac{-m z_g}{(m - X_{\dot{u}})}$	0.0909	0.0550	0.0959	0.3102
$\alpha_3 = \frac{(W-B)\sin(\theta)}{(m - X_{\dot{u}})}$	−2.5098	−2.8987	−2.4622	−2.1622
$\alpha_4 = \frac{X_{uuu}}{(m - X_{\dot{u}})}$	−8.5937	−7.4594	−8.6492	−7.4957
$\alpha_5 = \frac{X_{u|u|}}{(m - X_{\dot{u}})}$	−22.3129	−18.2884	−22.4870	18.2994
$\alpha_6 = \frac{X_u}{(m - X_{\dot{u}})}$	−32.7171	−29.7355	−32.8517	−29.5699
$\alpha_7 = \frac{X_{wq}}{(m - X_{\dot{u}})}$	−7.1061	−16.1337	−7.0680	−13.1852
$\alpha_8 = \frac{X_{vr}}{(m - X_{\dot{u}})}$	−13.5405	−12.7996	−13.5564	−12.8060
$\alpha_9 = \frac{X_{\psi|\psi|}}{(m - X_{\dot{u}})}$	–	–	–	–
$\alpha 10 = \frac{X_\psi}{(m - X_{\dot{u}})}$	–	–	–	–
$\alpha 11 = \frac{X_{\text{static}}}{(m - X_{\dot{u}})}$	–	–	–	–
$\beta_1 = \frac{(Y_{\dot{r}} - m x_g)}{(m - Y_{\dot{v}})}$	0.0133	0.0135	0.0133	0.0133
$\beta_2 = \frac{m z_g}{(m - Y_{\dot{v}})}$	0.0029	0.0031	0.0029	0.0029
$\beta_3 = \frac{Y_{v|v|}}{(m - Y_{\dot{v}})}$	0.0444	0.0173	0.0480	0.0094
$\beta_4 = \frac{Y_v}{(m - Y_{\dot{v}})}$	−0.0364	−0.0722	−0.0367	−0.0552
$\beta_5 = \frac{Y_p}{(m - Y_{\dot{v}})}$	0.0005	0.0004	0.0005	0.0004
$\beta_6 = \frac{Y_q}{(m - Y_{\dot{v}})}$	−0.0001	0.0003	0.0000	0.0001
$\beta_7 = \frac{Y_r}{(m - Y_{\dot{v}})}$	0.0008	0.0016	0.0007	0.0013
$\beta_8 = \frac{Y_{\psi|\psi|}}{(m - Y_{\dot{v}})}$	–	–	–	–
$\beta_9 = \frac{Y_\psi}{(m - Y_{\dot{v}})}$	–	–	–	–
$\beta_{10} = \frac{Y_{\text{static}}}{(m - Y_{\dot{v}})}$	–	–	–	–
$\gamma_1 = \frac{(Z_{\dot{q}} - m x_g)}{(m - Z_{\dot{w}})}$	−0.0059	−0.0062	−0.0058	−0.0061
$\gamma_2 = \frac{Z_{w|w|}}{(m - Z_{\dot{w}})}$	−0.0138	−0.0186	−0.0094	−0.0038
$\gamma_3 = \frac{Z_w}{(m - Z_{\dot{w}})}$	−0.0347	−0.9837	−0.0372	−0.7185
$\gamma_4 = \frac{Z_q}{(m - Z_{\dot{w}})}$	−0.0011	0.0044	−0.0010	−0.0083
$\gamma_5 = \frac{Z_r}{(m - Z_{\dot{w}})}$	0.0001	−0.0032	0.0001	−0.0028
$\gamma_6 = \frac{(W-B) + Z_{\text{static}}}{(m - Z_{\dot{w}})}$	0.0016	0.0020	0.0015	0.0020

Note that the values of the parameters are not pure hydrodynamic, hydrostatic and mass coefficients as the environmental and external forces are overlaid within them

gations in sway and heave velocities are negligibly smaller due to error counteraction during the velocity fluctuations. Table 4 presents the Root Mean Squared (RMS) errors [30] of baseline models in comparison with actual measurements from the DVL-bottom-track-aided INS. Good correlations were observed from all models with RMS errors less than 0.13, 0.03 and

$0.03\,\mathrm{m\,s^{-1}}$ for u, v and w. In comparison, as given in Table 1, the RMS uncertainty of surge, sway and heave velocity estimations from a DVL-water-track-aided INS is $0.3\,\mathrm{m\,s^{-1}}$, GPS-aided INS is $0.05\,\mathrm{m\,s^{-1}}$ and DVL-bottom-track-aided INS is $0.001\,\mathrm{m\,s^{-1}}$ [31,32].

The difference between velocity prediction uncertainties of the models identified using RLS and PEM
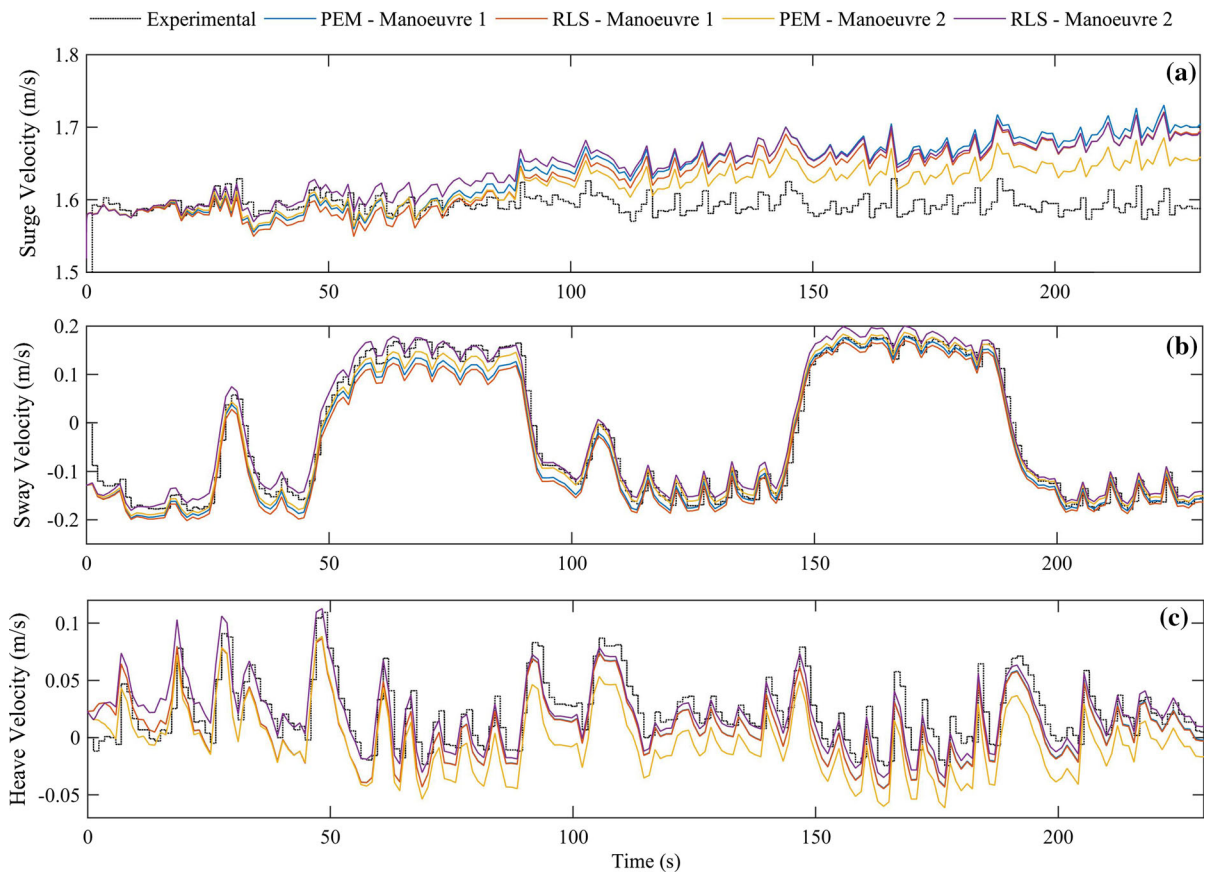
Fig. 5 Comparison between the baseline models and experimental velocities of the AUV in **a** x, **b** y and **c** z directions for the Lake Trevallyn field tests

Table 4 Accuracies of the vehicle velocity predictions from the four baseline models (i.e. models identified with RLS and PEM techniques, with each technique processed twice utilising ID Manoeuvres 1 and 2) compared to velocity measurements from the DVL-aided INS

Identification technique	Manoeuvre	RMS error compared to actual measurements (m s^{-1})		
		Surge velocity	Sway velocity	Heave velocity
RLS	ID Manoeuvre 1	0.13	0.03	0.02
	ID Manoeuvre 2	0.13	0.02	0.02
PEM	ID Manoeuvre 1	0.13	0.03	0.02
	ID Manoeuvre 2	0.12	0.02	0.03

are negligibly small (see Table 4). That is, both identification algorithms are equally capable of estimating the parameters of the model defined by Eqs. (9), (10) and (11). The initial parameter values were set to 1 in both techniques in order to preserve the assumption that the initial guesses of the parameters are unknown. Dependency of the parameters estimation accuracy on the initial values was evaluated by repeating the RLS and PEM estimation algorithms with initial values being set to previously identified parameters. Negligibly small variations of the parameter values were observed (i.e. less than 0.5%). Therefore, the estimated parameters
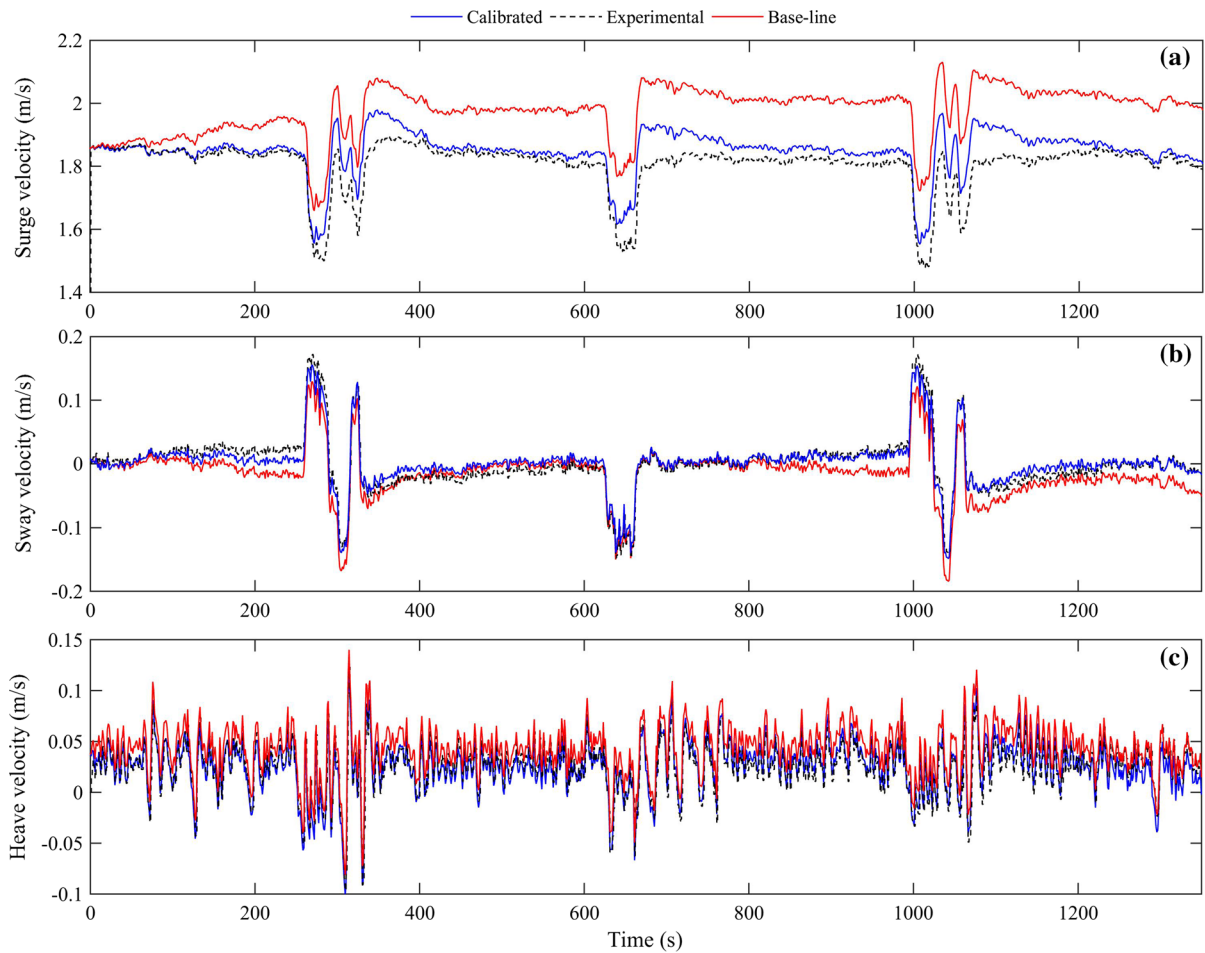
Fig. 6 Comparison of the baseline and calibrated model-aided INS velocities in **a** x, **b** y and **c** z directions against those from the DVL-aided INS for the Lake Ohau runs 2 and 3

are independent of the initial values. This is likely to be as a result of the utilised identification manoeuvres that stimulate the vehicle dynamics in all motion modes.

The parameter estimation was repeated for both ID Manoeuvres 1 and 2 to investigate the variation of the estimated parameters with the utilised dataset. As seen from Fig. 5, models obtained by processing both datasets perform well with a maximum RMS difference of 0.01 m s^{-1} (see Table 4). The RLS and PEM algorithms were able to process an 862-s long dataset with computation times of 12 and 10 s utilising an Intel Core i7-4470 3.40 GHz central processing unit. That is, the measurement data can be processed in rates of 74 and 62 Hz, respectively. Real-time measurement sampling rate of the AUV is around 25 Hz. Therefore, either of

the two algorithms are deemed to be feasible for real-time or near-real-time estimation.

Given that all four baseline models are equally capable, the model parameters obtained from RLS technique by processing ID Manoeuvre 1 were utilised for the discussion hereinafter. The baseline model-aided INS solution was obtained by fusing the vehicle velocities from the RLS baseline model with unaided-INS acceleration measurements. A Kalman filter based data fusion algorithm developed according to Farrell [33] was utilised for INS aiding. The baseline model-aided INS was tested for the lawn mower pattern run in Lake Ohau (AUV runs 5–8) to investigate the performance in different environments (recall Fig. 2b). Figure 6a–c compares u, v and w velocities of the vehicle from baseline model-aided INS against those measured by the

AUV's DVL-aided INS. The sudden peaks and dips at the time periods of 300, 650 and 1050 s were a result of the 180° heading turns of the vehicle at the end of each straight line run. The RMS errors between the baseline model-aided INS and experimentally measured DVL-aided INS were 0.15, 0.02 and 0.02 m s^{-1} for u, v and w, respectively. The AUV's on-board ADCP measured an averaged background water current magnitude of around 0.1 m s^{-1} in the Lake Ohau test site. According to the WVAM method [11], the difference between the actual vehicle velocities and those simulated by a baseline model that represents a calm environment provides the velocities of the water column around the AUV. Although this difference is reduced when the baseline model is fused with INS acceleration measurements that are measured relative to the inertial space, the observed difference between the two is as result of the water currents in Lake Ohau.

The baseline model was calibrated by running the calibration algorithm for AUV runs 1–4 in Lake Ohau. The solid blue lines in Fig. 6 show the velocity from the calibrated model-aided INS for AUV runs 5–8. A significant improvement is that RMS errors compared to actual measurements have reduced to 0.04, 0.01 and 0.01 m s^{-1} for respective velocities in surge, sway and heave directions. That is an improvement of 73, 50 and 50% in each of the three directions, respectively.

The baseline model-aided INS surge velocity prediction diverges with time compared to DVL-aided INS solution due to the accumulation of error. However, the surge velocity is accurately estimated by the calibrated model-aided INS for the entire duration of the mission. Out of the three, the heave velocity component delivered the most accurate replication of the actual velocity of the AUV. Although the velocity prediction in z direction is not critical for localisation as the vehicle depth and depth rates can be accurately measured with the pressure sensor, it can be used as a backup for emergency situations.

There is an uneven divergence between the actual and calibrated sway velocities (Fig. 6b). Consistently, this difference is observed at one side of the four lawn-mower pattern straight lines, i.e. at the right-hand side of the bathymetry shown in Fig. 2c. This could be due to strong underwater currents of around 0.15 m s^{-1} present near the inflow point caused by the Hopkins and Dobson Rivers [23]. This discrepancy gets larger as the distance gets smaller. Therefore, a water column velocity measurement method could be integrated together

with the model predicted vehicle velocities in order to improve the accuracy of the localisation solution of the AUV when DVL aiding is unavailable for longer time intervals [9,10].

Figure 7a compares the two-dimensional (2D) localisation solutions computed using the measured vehicle velocities (i.e. the actual vehicle path) and those estimated using the baseline model for the pitch and yaw plane zig-zag manoeuvres conducted in Lake Trevallyn site. Note that the AUV paths are plotted in a local coordinate system. The baseline model predicted localisation solution was within the 1.5% of the distance travelled uncertainty range. Therefore, the estimated baseline model is deemed accurate to predict the vehicle position with an uncertainty margin of 1.5% of the distance travelled when the AUV is operating under similar environmental forcings.

Figure 7b compares the 2D localisation solutions of the AUV for Lake Ohau runs 5–8 computed using the measured DVL-aided INS velocities and those from the baseline and calibrated model-aided INSs. The baseline model-aided INS over predicts the surge velocity of the AUV by approximately 0.15 m s^{-1}, resulting in a deviated vehicle position derivation compared to the actual path. However, this position error is counteracted during the opposite directions runs of the lawn-mower pattern mission. The over prediction of the surge velocity is significantly reduced in the calibrated model providing a more accurate localisation solution.

Figure 7c plots the localisation errors (i.e. the difference between the DVL-aided and model-aided INS vehicle positions) for baseline and calibrated models against the AUV's travel distance for the Lake Ohau mission. The fluctuations in the localisation errors are due to the error counteraction during the opposite direction runs. Three different uncertainty margins are indicated by grey shaded areas with dark grey representing the localisation error level of 0.1% of the distance travelled. Grey and light grey zones show respective error levels of 1.5 and 4.0% of the distance travelled. The localisation solution from the baseline model-aided INS was outside of the 1.5% band, but was generally within the 1.8% of the distance travelled margin. The positioning uncertainty is generally within 1.5% level when the model is calibrated to the operational environment.

The localisation accuracy of the *Gavia* AUV with Kearfott T24 INS when DVL aiding is available is within 0.1% of the distance travelled, i.e. region shaded
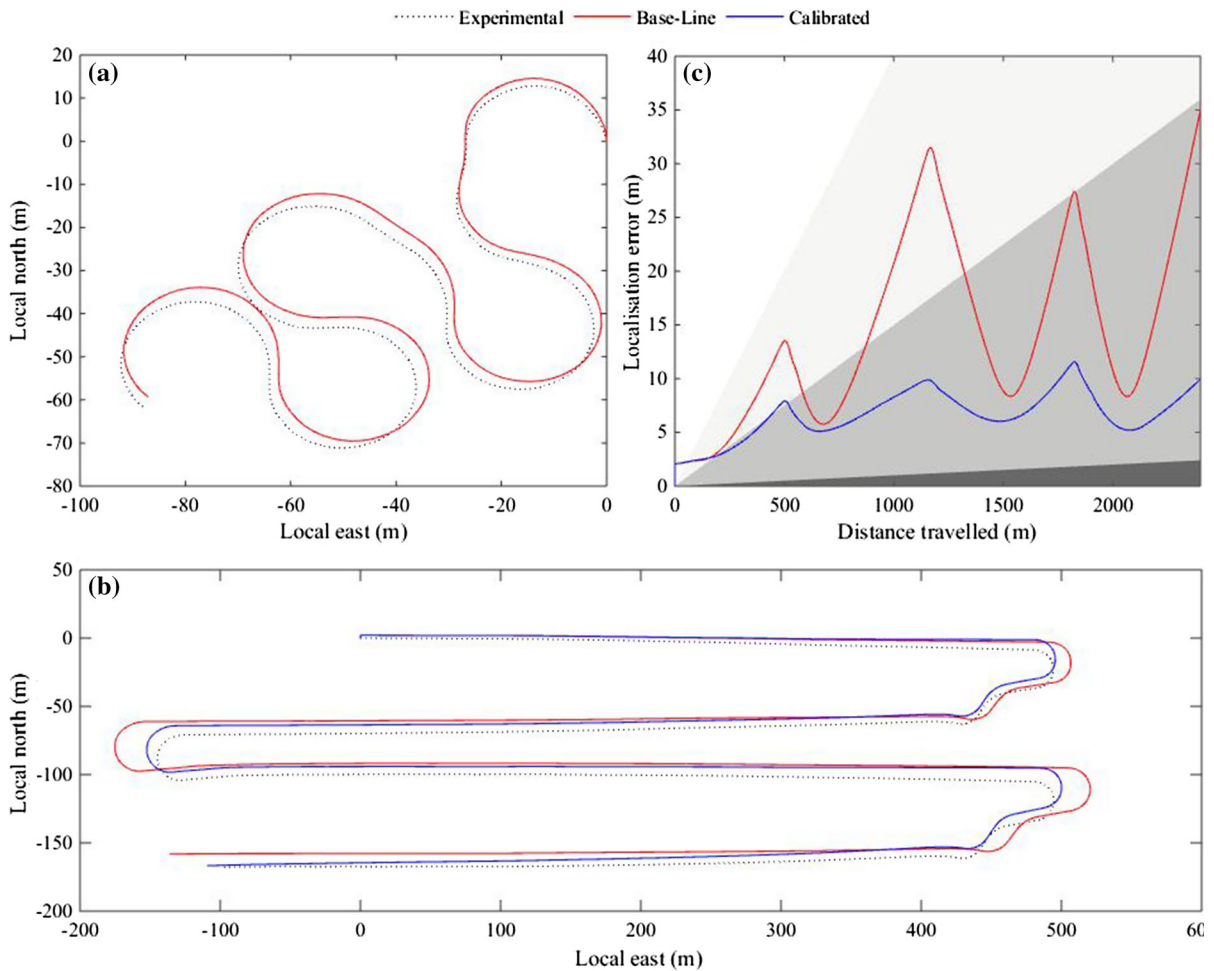
Fig. 7 a Two-dimensional AUV paths of Lake Trevallyn manoeuvres derived from the actual vehicle velocities (i.e. experimental), and baseline model predicted velocities plotted in a local coordinate system. **b** Actual and model predicted (i.e. baseline model and calibrated model) localisation solutions of Lake Ohau runs 5–8. **c** Comparison of the localisation errors (i.e. the difference between the actual and model predicted vehicle positions) from baseline and calibrated models. Dark grey area indicates the 0.1% of the distance travelled localisation error level (i.e. positioning uncertainty of a typical DVL-bottom-track-aided-INS), while grey and light grey regions show that of 1.5 and 4.0% (i.e. the localisation error level of an DVL-water-track-aided INS)

in dark grey [34]. However, according to the published specifications, the DVL-water-track-aided Kearfott T24 INS (i.e. when DVL-bottom-track is unavailable) has a time root mean squared localisation uncertainty of 1852 m (i.e. 1 nm) per 8 hours [32]. Assuming a forward speed of $1.6\,\mathrm{m\,s^{-1}}$, this yields a positioning error of around 4.0% of the distance travelled (i.e. region shaded in light grey). A calibrated model-aided INS could limit the positioning uncertainty to around 1.5% of the distance travelled for a typical AUV mission.

6 Real-time model identification

6.1 Real-time parameter calibration

In highly dynamic environments, the parameters of the mathematical model fluctuate with time due to environmental and external forcing. The objective of the real-time model calibration algorithm is to generate a mathematical model that continuously updates to provide the vehicle motion response in the present operational environment, especially in highly dynamic environments.

Table 5 The variation of the averaged difference between the actual and simulated accelerations with the forgetting factor for Lake Trevallyn and Ohau runs

Forgetting factor	Averaged difference between actual and simulation accelerations (m s $^{-2}$)					
	Lake Trevallyn test			Lake Ohau test		
	Surge	Sway	Heave	Surge	Sway	Heave
0.90	1.49×10^{-8}	2.59×10^{-7}	9.19×10^{-9}	3.14×10^{-8}	1.59×10^{-8}	2.11×10^{-8}
0.95	1.84×10^{-7}	1.93×10^{-6}	1.13×10^{-7}	3.55×10^{-8}	3.67×10^{-7}	4.83×10^{-8}
1.00	1.37	4.60×10^{-3}	3.81×10^{-3}	4.18×10^{-3}	1.55×10^{-3}	1.61×10^{-3}

The procedure outlined in Sect. 5.2 was employed for real-time parameter calibration. However, in order to identify the variation of parameters in a dynamic environment, data from preceding measurements have to be forgotten/discarded as new data arrives and the successive measurements should contain a higher weighting in the estimation process. Therefore, the performance of the real-time calibration model for different data processing set lengths was investigated by testing for forgetting factors of 1.00, 0.95 and 0.90; i.e. an infinite length, a time period of 20 and 10 s, respectively.

6.2 Performance analysis and discussion

In order to verify whether the mathematical model provided by the real-time model calibration method precisely represents the hydrodynamic characteristics of the AUV, the real-time algorithm was tested using a horizontal heading angle zig-zag manoeuvre conducted in Lake Trevallyn (i.e. the first 260 s of the ID Manoeuvre 1 shown in Fig. 3) and a straight line run conducted in Lake Ohau (i.e. AUV Run 1 shown in Fig. 2b). Parameters that are being updated in real time were used in the simulation model to determine the vehicle linear accelerations along surge, sway and heave directions and were compared against those measured by the vehicle INS. The maximum discrepancy between the two was observed in the surge acceleration.

Table 5 presents the averaged difference between the actual and simulated accelerations for forgetting factors of 1.00, 0.95 and 0.90. The accuracy of the real-time model is extremely low when the forgetting factor was set to 1 in order to disable the forgetting effect and to process the entire data series from the first to the last measurement. On the other hand, the averaged percentage differences for the Lake Trevallyn and Lake Ohau runs for the forgetting factors of both 0.90

and 0.95 were less than 1%. Thus, the accuracies of the mathematical models identified using the real-time algorithm increased significantly after enabling the forgetting effect. It can be concluded that the smaller the forgetting factor is (i.e. the shorter the length of the data series being processed) the higher is the accuracy.

7 Limitations and future work

The model identification algorithms presented in this article utilise the roll, pitch and yaw rates and accelerations as the control command inputs instead of the control surface angles to create a simplified 3-DOF model of the vehicle. Although the use of this model presents a major limitation for using on AUVs without accurate sensors to measure vehicle orientations, it would be widely applicable for most commercially available AUVs on the market today.

Although the calibration method can be utilised to adjust a baseline model of an AUV for different configurations, this was not experimentally verified in this work. Authors expect to investigate this by testing the algorithm for different configurations of the *Gavia* AUV. Furthermore, it is anticipated to link the model predicted vehicle velocities with the non-acoustic water column velocity estimation method (i.e. the WVAM method) previously developed by the authors [10] in order to accurately estimate the vehicle velocities over ground for INS aiding.

One of the key advantages of the mathematical model identification and calibration algorithms is that they could be applied to any torpedo-shaped AUV (e.g. *REMUS*, *Iver*, *Bluefin*, *Explorer*, etc.) in any configuration. Authors have utilised this algorithm to successfully identify the mathematical models of an *Iver III* AUV and a *Gavia* AUV with different module configurations.

8 Conclusions

This study presents a system identification algorithm to determine the linear and nonlinear parameters of an AUV mathematical model utilising the RLS and PEM optimisation methods. A baseline model that represents the dynamics of the *Gavia* AUV in a calm water environment was developed. The estimated baseline model accurately predicted the vehicle velocities in three dimensions when the vehicle and environmental conditions are similar to those represented by the baseline model. Model accuracy decreases when the operational environment is different. A novel technique was developed in this study to calibrate the parameters within the baseline model to different environmental conditions by conducting a calibration mission in the new environment. The accuracy of the velocity measurements from the calibrated model was substantially greater than those from the baseline model for the tested scenarios with a minimum velocity prediction improvement of 50%. The calibrated model is able to compute the position of the AUV within an uncertainty range of 1.5% of the distance travelled. It is hypothesised that this uncertainty could be further reduced by incorporating the model predicted vehicle speeds obtained through a water column velocity estimation method. In comparison, the uncertainty of a DVL-aided INS is around 0.1% of the distance travelled and that of a DVL-water-track-aided INS is around 4% (assuming a forward speed of 1.6 m s^{-1}).

The algorithm was extended to real-time parameter calibration and the extended algorithm was tested at two field sites with different environmental conditions; i.e. in a quiescent lake with relatively flat seabed, and in a more dynamic water column with rough and unstructured bathymetry. The performance of the real-time calibration model for different processing data set lengths were investigated by testing for forgetting factors of 1.00, 0.95 and 0.90. The smaller the forgetting factor is (i.e. the shorter the length of the data series being processed), the higher is the accuracy.

The long-term objective of this work is to predict the three-dimensional velocity vector of the AUV in order to localise the vehicle when velocity over ground measurements from the DVL are unavailable for INS aiding.

References

1. Mcleod, D., Jacobson, J.R., Tangirala, S.: Autonomous inspection of subsea facilities-Gulf of Mexico trials. In: Offshore Technology Conference Offshore Technology Conference (2012)
2. Curtin, T.B., Bellingham, J.G., Catipovic, J., Webb, D.: Autonomous oceanographic sampling networks. Oceanography **6**(3), 86–94 (1993)
3. Paull, L., Saeedi, S., Seto, M., Li, H.: AUV navigation and localization: a review. IEEE J. Ocean. Eng. **39**(1), 131–149 (2014)
4. Hegrenæs, Ø., Berglund, E.: Doppler water-track aided inertial navigation for autonomous underwater vehicle. In: IEEE OCEANS 2009-EUROPE pp. 1–10 (2009)
5. Jalving, B., Gade, K., Hagen, O.K., Vestgard, K.: A toolbox of aiding techniques for the HUGIN AUV integrated inertial navigation system. In: OCEANS 2003. Proceedings pp. 1146–1153. IEEE (2003)
6. Medagoda, L., Jakuba, M.V., Pizarro, O., Williams, S.B.: Water column current profile aided localisation for autonomous underwater vehicles. In: OCEANS 2010 IEEE-Sydney pp. 1–10. IEEE (2010)
7. Hegrenaes, O., Berglund, E., Hallingstad, O.: Model-aided inertial navigation for underwater vehicles. In: 2008 IEEE International Conference on Robotics and Automation. ICRA 2008, pp. 1069–1076. IEEE (2008)
8. Jayasiri, A., Gosine, R.G., Mann, G.K., McGuire, P.: AUV-based plume tracking. J. Control Sci. Eng. **2016**, 12 (2016)
9. Hegrenæs, Ø., Hallingstad, O.: Model-aided INS with sea current estimation for robust underwater navigation. IEEE J. Ocean. Eng. **36**(2), 316–337 (2011)
10. Randeni, S.A.T., Forrest, A.L., Cossu, R., Leong, Z.Q., King, P.D., Ranmuthugala, D.: Autonomous underwater vehicle motion response: a nonacoustic tool for blue water navigation. Mar. Technol. Soc. J. **50**(2), 17–26 (2016)
11. Randeni, S.A.T., Forrest, A.L., Cossu, R., Leong, Z.Q., Ranmuthugala, D.: Estimating flow velocities of the water column using the motion response of an Autonomous Underwater Vehicle (AUV). In: OCEANS '15 MTS/IEEE, Washington D.C. IEEE (2015)
12. Ananthakrishnan, P.: AUV hydrodynamics in shallow water during adverse weather conditions. In. DTIC Document (1998)
13. Randeni, S.A.T., Leong, Z., Ranmuthugala, D., Forrest, A., Duffy, J.: Numerical investigation of the hydrodynamic interaction between two underwater bodies in relative motion. Appl. Ocean Res. **51**, 14–24 (2015)

14. Polis, C., Ranmuthugala, D., Duffy, J., Renilson, M.: Enabling the prediction of manoeuvring characteristics of a submarine operating near the free surface. In: Pacific 2013 International Maritime Conference: The Commercial Maritime and Naval Defence Showcase for the Asia Pacific, p. 281. Engineers Australia (2013)

15. Hong, E.Y., Meng, T.K., Chitre, M.: Online system identification of the dynamics of an autonomous underwater vehicle. In: Underwater Technology Symposium (UT), 2013 IEEE International, pp. 1–10. IEEE (2013)

16. Song, F., An, P.E., Folleco, A.: Modeling and simulation of autonomous underwater vehicles: design and implementation. IEEE J. Ocean. Eng. **28**(2), 283–296 (2003)

17. Dash, A.K., Nagarajan, V., Sha, O.P.: Bifurcation analysis of a high-speed twin-propeller twin-rudder ship maneuvering model in roll-coupling motion. Nonlinear Dyn. **83**(4), 2035–2053 (2016)

18. Liang, X., Li, Y., Peng, Z., Zhang, J.: Nonlinear dynamics modeling and performance prediction for underactuated AUV with fins. Nonlinear Dyn. **84**(1), 237–249 (2016)

19. Marco, D.B., Martins, A., Healy, A.J.: Surge motion parameter identification for the NPS Phoenix AUV. In: DTIC Document(2005)

20. Yan, Z., Wu, D., Zhou, J., Hao, L.: Recursive Subspace Identification of AUV dynamic model under general noise assumption. Math. Probl. Eng. **2014**, 547539 (2014)

21. Fossen, T.I.: Handbook of Marine Craft Hydrodynamics and Motion Control. Wiley, Hoboken (2011)

22. Þorgilsson, H.: Control of a small undermanned underwater vehicle using zero optimizing controllers. Master's thesis, Department of Electrical and Computer Engineering, University of Iceland, Reykjavík, Iceland (2006)

23. Cossu, R., Forrest, A., Roop, H., Dunbar, G., Vandergoes, M., Levy, R., Stumpner, P., Schladow, S.: Seasonal variability in turbidity currents in Lake Ohau, New Zealand, and their influence on sedimentation. Mar. Freshwater Res. (2015). https://doi.org/10.1071/MF15043

24. Steel, V.: Investigation into the Effect of Wave Making on a Submarine Approaching the Free Surface. University of Tasmania, Hobart (2010)

25. Newman, J.N.: Marine Hydrodynamics. MIT press, Cambridge (1977)

26. Fossen, T.I.: Marine control systems: guidance, navigation and control of ships, rigs and underwater vehicles. Mar. Cybern. (2002)

27. Abkowitz, M.A.: Lectures on ship hydrodynamics-Steering and manoeuvrability. In. Hydro- and Aerodynamic's Laboratory, Lyngby, Denmark (1964)

28. Ljung, L.: System Identification: Theory for the User. Prentice Hall PTR, Upper Saddle River (1999)

29. Sun, X.J., Shi, J., Yang, Y.: Neural networks based attitude decoupling control for AUV with X-Shaped fins. In: Wang, T., Guo, H., Zuo, D., Xu, J. (eds.) Advanced Materials Research, pp. 222–228. Trans Tech Publ (2013)

30. Devore, J.L.: Probability and Statistics for Engineering and the Sciences. Cengage Learning, Boston (2011)

31. Alameda Jr, W.: Seadevil-A totally integrated inertial navigation system (INS) solution. In: Proceedings of the 2002 Underwater Intervention Symposium (2002)

32. Kearfott Corporation: Kearfott sea navigation unit data sheet http://www.kearfott.com/wp-content/uploads/2016/09/Kearfott_SeaNav.pdf (2016). Accessed 6th of January (2017)

33. Farrell, J.: Aided navigation: GPS with high rate sensors. McGraw-Hill, Inc, New York City (2008)

34. Hiller, T., Reed, T., Steingrimsson, A.: Producing chart data from interferometric sonars on small AUVs. Int. Hydrogr. Rev. (6), 43–50 (2011)